Chapter 5

Chemical and Spatial Analysis of Protein Loaded PLGA Microspheres for Drug Delivery Applications.

5.1 Introduction

In recent years there has been an increase in the availability and development of protein and peptide controlled release therapeutics, such as microspheres for sustained perenteral delivery[1-5]. Such applications include vaccination[2, 6-8] and drug delivery[9-13], for periods of up to 6 months. Understanding the surface and the bulk chemical composition of such microspheres provides a greater insight into the production process and may also contribute to the understanding of the contribution of structure to the nature of the drug release kinetics observed.

As described in Chapter 1 the molecular characterisation of such polymeric drug delivery formulations is crucial to provide an understanding of release from such microspheres. This chapter therefore is concerned with the full physical and chemical characterisation of both the surface and bulk of a protein loaded PLGA microsphere formulation with a range of complementary techniques. The technique of ToF-SIMS has been extensively used to study pharmaceutical systems[14-19]. The utility of ToF-SIMS comes from the ability to provide high surface specificity chemical information with high depth resolution (~1-2 nm). AFM is a complementary technique to ToF-SIMS providing nm lateral resolution of the surface topography which has been previously been applied to microspheric systems[20, 21] for surface topography characterisation.

ToF-SIMS depth profiling has been used to analyse biomedically relevant thin films[17, 19] to elucidate the spatial distribution of various constituents within such systems through thickness in order to improve the properties of the formulation. Due to the topography encountered with microsphere structure this has not been as widely applied to the study of microspheres. This is especially true for dual beam depth profiling whereby the sputter and analysis beams are often mounted

opposite one another with each ion beam at a 45° elevation. Dual beam depth profiling therefore necessitates sample stage rotation and realignment of the sample stage between cycles of sputtering and analysis. This is in order to have both the sputter and analysis beam focussed on the same analysis region of the microsphere with alignment remaining a challenge. In this work ToF-SIMS is used to chemically characterise the surface and bulk with imaging using the burst alignment mode described in depth in Chapter 2.

The analysis of the bulk is crucial to the characterisation of pharmaceutical microsphere systems as the distribution of drug within the microsphere will determine the release characteristics. Confocal Raman microscopy whereby a plane within a transparent sample is focussed on and Raman spectra mapped for that focal plane providing a ~1 µm depth resolution was used for non-destructive bulk characterisation. As described in Chapter 2 the Raman mapping provides vibrational spectra through the collection of scattered light to map the chemistry from within the focal plane selected. It has been used in conjunction with ToF-SIMS of sectioned microspheres in this chapter in order to characterise the bulk distribution of protein and polymer. The results of this characterisation should allow for the distribution of constituent chemistries to be related back to the production process. Raman mapping has previously been applied to pharmaceutical systems including drug loaded polymeric microspheres[22, 23], thin polymer films[18, 19, 24] and tablet compound identification[25], specifically using multivariate methods of analysis [26-28].

The use of these techniques allows for a 3D understanding of the drug delivery method and serves to illustrate the complementary use of surface analytical techniques for full characterisation of a PLGA microsphere drug delivery system. A double emulsion solvent evaporation process is used to produce the microspheres used in this study. The protein lysozyme is used as a model drug for release from within the PLGA microspheres. This model is produced and characterised for nominally produced microspheres which will be incorporated within a tissue engineering scaffold for bone repair providing mechanical support at the site of non-unified bone fractures[29, 30]. Microspheres embedded within such a scaffold release the protein BMP2 to stimulate osteogenesis[31]. As the scaffold

and microspheres degrade the protein therapeutic, having stimulated bone repair, will gradually transfer the load on the fracture from the scaffold to the new bone. In this chapter a complementary approach is used to provide a detailed understanding of component distribution within a PLGA microspheric controlled release formulation for the delivery of protein drug. The full characterisation of such microspheres provides valuable information that allows for improvements to be made in the microsphere fabrication process, ultimately improving the therapeutic properties.

The aims of this chapter are to demonstrate the full characterisation of a complex water in oil in water double emulsion (w/o/w) to allow for inferences to be made as to how the production process affects the distribution of chemical constituents. This is done to expand on the work previously done with ToF-SIMS of particles and to improve the lateral resolution attainable with ToF-SIMS chemical imaging of samples with topography.

5.2 Experimental

Custom polymerised PLGA (56 kDa) was obtained from Lakeshore Biomaterials (Birmingham, Alabama, USA) consisting of a molar ratio of 85:15 of DL-lactic acid and glycolic acid respectively. Polyvinyl alcohol (PVA, 87-89 % hydrolysed), hen egg white lysozyme and all solvents were purchased from Sigma Aldrich (Dorset, UK). The microspheres were produced using a w/o/w solvent evaporation method containing 1.5%, 3%, 5% and 10% (w/v) lysozyme described in previous work[32, 33] a schematic representation is shown in Figure 5.1. A water in oil emulsion was established with the concentrations of lysozyme described dissolved in 300 µl of phosphate buffered saline (PBS, water phase) added to 5 ml of PLGA dissolved in dichloromethane (DCM, oil phase) and vortex mixing was applied. Before the emulsion can separate 5 ml of PVA surfactant is added and vortex mixing resumed. The microspheres are then placed in a hardening bath with an excess of 2% (w/v) PVA solution for a period of 3 h under gentle stirring to allow the DCM to evaporate. The particles were extracted by vacuum filtering to isolate the resultant microspheres which were then freeze dried for 24 h.

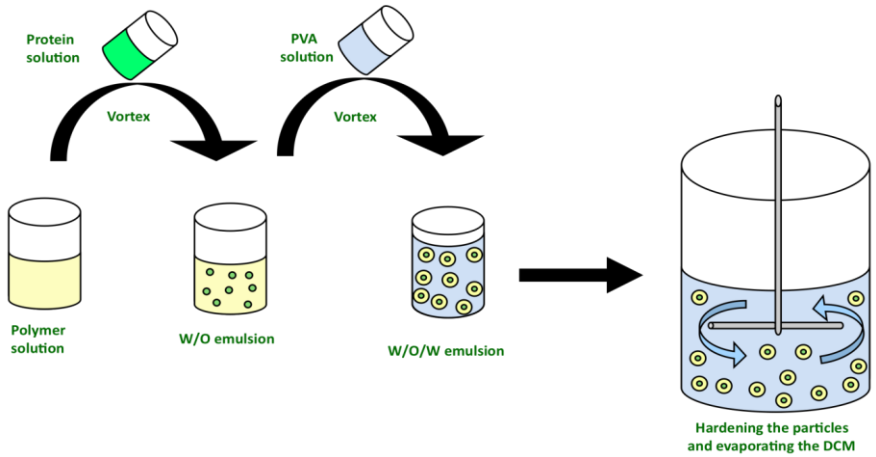

Figure 5.1 Schematic of a double emulsion production method.

ToF-SIMS data was acquired using a ToF-SIMS IV (ION-TOF GmbH, Munster, Germany) described in Chapter 2. The samples were loaded by sprinkling on double sided tape attached to aluminium blocks affixed into the ToF-SIMS stage. For imaging studies 25 keV Bi_3^+ primary ions were used for analysis using a 256 × 256 pixel raster while ensuring the total ion fluence did not exceed the static limit. For surface sputtering the SIMS stage was rotated after acquisition using Bi_3^+ using the Eucentric capability of the Escosy stage control program, 20 keV C_{60}^{2+} primary ions were used to sputter a 1 mm area for 28 s then the stage was rotated again for analysis of the sputtered surface, this process was repeated four times.

Scanning electron microscopy (SEM) was undertaken using a JEOL JSM-6060LV scanning electron microscope. An acceleration voltage of 10 keV was used with no visible damage imposed during analysis. Samples were prepared by sprinkling microspheres onto an adhesive carbon tab affixed to an aluminium SEM stub (Agar Scientific, Essex, UK) and gold coating for 2 min at 13 mA using a Leica EM SCD050 gold coater (Leica Microsystems GmbH, Wetzlar, Germany).

Raman spectra were acquired using a WITec CRM200 (WITec Instruments Corp. Ulm, Germany) equipped with a 532 nm laser source, with the laser line suppressed by an edge filter. This laser excitation source was focused using a 100x objective and the scattered light was collected using the same objective in an 180^o backscatter regime. The Stokes shifted Raman scatter was dispersed using a

600 grooves/mm grating onto a charged coupled device (CCD), providing a spectral resolution of ~8 cm^{-1}.

Raman maps were acquired from between 20 and 30 µm beneath the sample surface at intervals of 1 µm. Each Raman map was acquired over an area of 40 µm x 40 µm and constructed using a serial mapping process. This involves the acquisition of spectra at defined points within an array using a CCD, and provides lateral and depth resolution of ~1 µm. The spectra were not subjected to any spectral corrections to correct for aberrations or artefacts; however, the inherent signal from thermal noise was subtracted from each spectrum.

AFM was undertaken using a Veeco MultiMode AFM (Cambridge, UK), Quantitative nanomechanical property mapping (QnM) mode was used in order to get maximal data from the scanning probe technique as it allows for properties such as the Young's modulus, adhesion and deformation to be measured while imaging at high resolution. An 8 µm area at the top of the microspheres were analysed before and after sputtering with C_{60}^{2+} primary ions. The techniques used in this chapter are summarised in Figure 5.2 below.

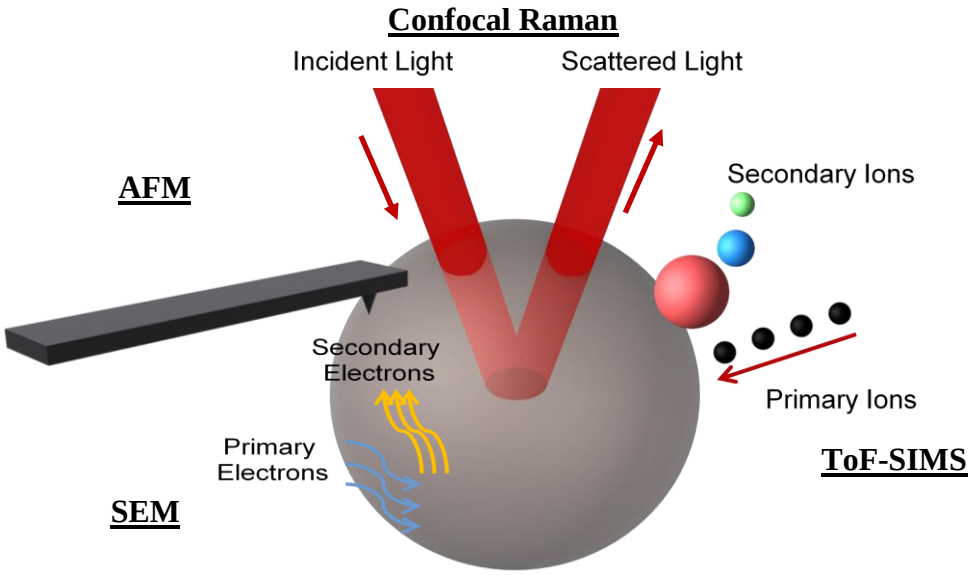

Figure 5.2 Schematic diagram of analytical methods applied to the microsphere samples.

5.3 Results and Discussion

SEM was employed to gain an understanding of the size distribution and surface topography of the lysozyme PLGA microspheres and representative data is shown in Figure 5.3. The majority of microspheres appear smooth and spherical with their size varying between 30 and 150 μm in diameter, as shown in Figure 5.3a. Figure 5.3b shows at greater magnification the surface structure of some microspheres. Pores at the surface of these microspheres measure from 2 to 11 μm in diameter and a ring like morphology around some pores but not others is observed. Some circular, pitted surface structures are also found at the surface in the absence of a visible pore. There appears to be no evidence of protein aggregates on the surface of the microspheres.

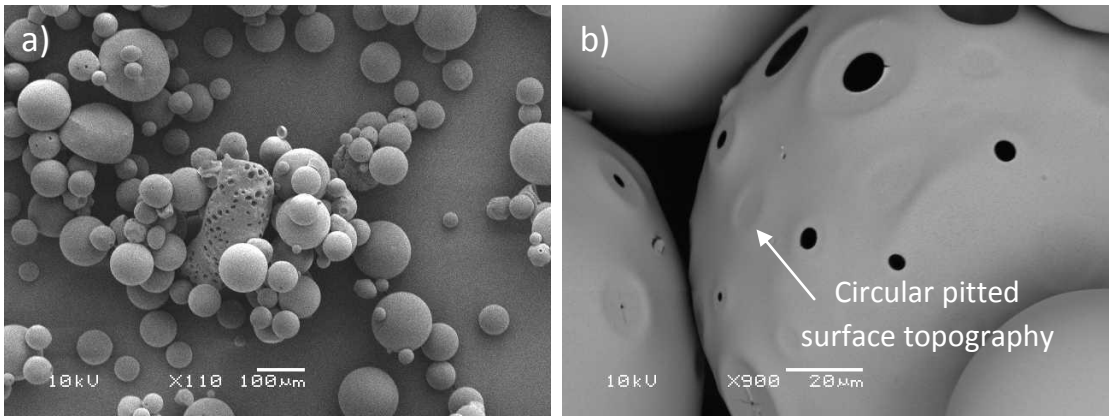

Figure 5.3 SEM analysis of w/o/w lysozyme PLGA microspheres shown at a) ×110 and b) ×900 magnification.

The range of the particle size distribution is as expected from the process of w/o/w production of the microspheres where a normal distribution of particle size is often observed[33]. Surface pores observed are likely to be formed on the inversion stage of the microemulsion where the PVA water phase which contains the protein is encapsulated within the PLGA oil phase. Those water droplets that are not fully encapsulated and are at or near the interface of the PLGA-rich oil droplets would be expected to produce the surface pores. The origin of the pitted circular surface topography is unknown but many of such features such as the two highlighted in Figure 5.3b appear to be near to surface pores.

An example of a negative ion ToF-SIMS spectrum of the PLGA lysozyme microspheres is shown in Figure 5.4. After careful review of the ToF-SIMS of the individual surfactant, polymer and protein controls and literature, diagnostic ions of each of the three components of the formulation may be distinguished in the ToF-SIMS analysis of the microspheres in Figure 5.4. Peaks observed at *m/z* 71/73, and *m/z* 87/89 correspond to $[M \pm H]^-$ and $[M+O \pm H]^-$ respectively, where M is the repeating unit of LA monomer ($C_3H_4O_2$) of the PLGA copolymer[34]. The base peak (most prominent) of the spectrum at *m/z* 59 is diagnostic of PVA and corresponds to the acetate anion CH_3COO^- which has previously been used as a diagnostic peak in a PLGA/ PVA system[15]. The high intensity of the acetate anion is derived from the unhydrolysed vinyl acetate monomers within the 87% hydrolysed PVA used is this study. For the hen egg white lysozyme, the diagnostic peaks of CN^- and CNO^- at *m/z* 26 and 42 derived from the peptide sequence were selected as these can only arise from the protein in this formulation. In addition, multivariate curve resolution (data not shown) which highlighted these peaks as being statistically significant and related specifically to the protein structure. The peaks selected are sufficiently intense to allow for the reconstruction of the spectra into an image format.

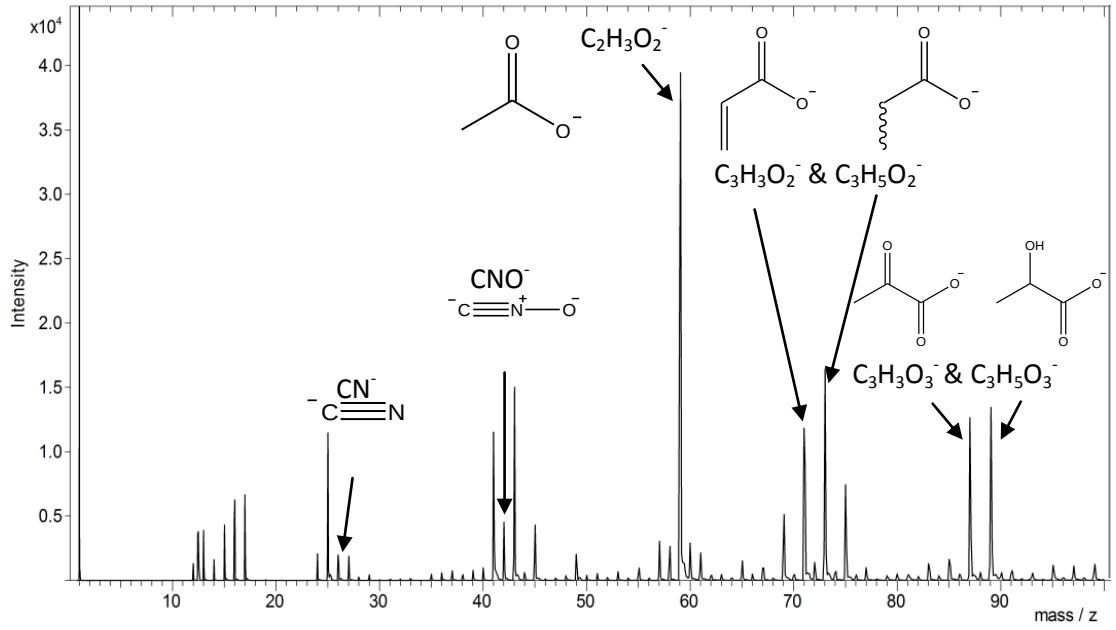

Figure 5.4 Negative ToF-SIMS spectrum of the surface of PLGA lysozyme microspheres from a mass of 0 to 100.

Using the diagnostic ions highlighted above, the ToF-SIMS spectra were reconstructed as images to understand the distribution of the PLGA, PVA and lysozyme at the surface of these microspheres. Figure 5.5 shows a ToF-SIMS image of the surface of a range of microspheres. Focusing attention to the main microsphere at the centre of the image, the ToF-SIMS image for PLGA is not continuous over the surface (Figure 5.5a). The reason for this is that the surface of the microsphere is coated with a discontinuous layer of PVA as illustrated in Figure 5.5b where discrete features as small as 700 nm in diameter may be distinguished. The thickness of the coverage of the PVA masks the underlying PLGA suggesting that it is greater than the sampling depth of the ToF-SIMS of circa 1 nm under the static conditions employed in the ToF-SIMS analysis. Many of the features within the PVA film are circular and ring-like with many discrete isolated islands of the surfactant on the surface of the microsphere. Similar features are seen on the surface of the other smaller microspheres within Figure 5.5b.

At the apex of the central microsphere in Figure 5.5, a surface pore is observed which is surrounded by an intense circular ring enriched in protein (Figure 5.5c). Again, the thickness of this overlayer appears to be greater than the 1 nm as no PLGA is detected in this region although there is evidence of the presence of PVA, particularly on the outer portion of the ring structure and also as a discrete intense feature at the bottom lip of the pore. There are also lower intensity protein signals detected and associated with the PVA surfactant discontinuous layer (particularly visible in the lower left hand side of the main microparticle and also on other microparticle surfaces in Figure 5.5c) but not on the bare PLGA surface. The overlay of all these three image sets in Figure 5.5d clearly demonstrates the ability of ToF-SIMS to discriminate for this particular formulation the different chemistries and their complex organisation on the microparticle surfaces.

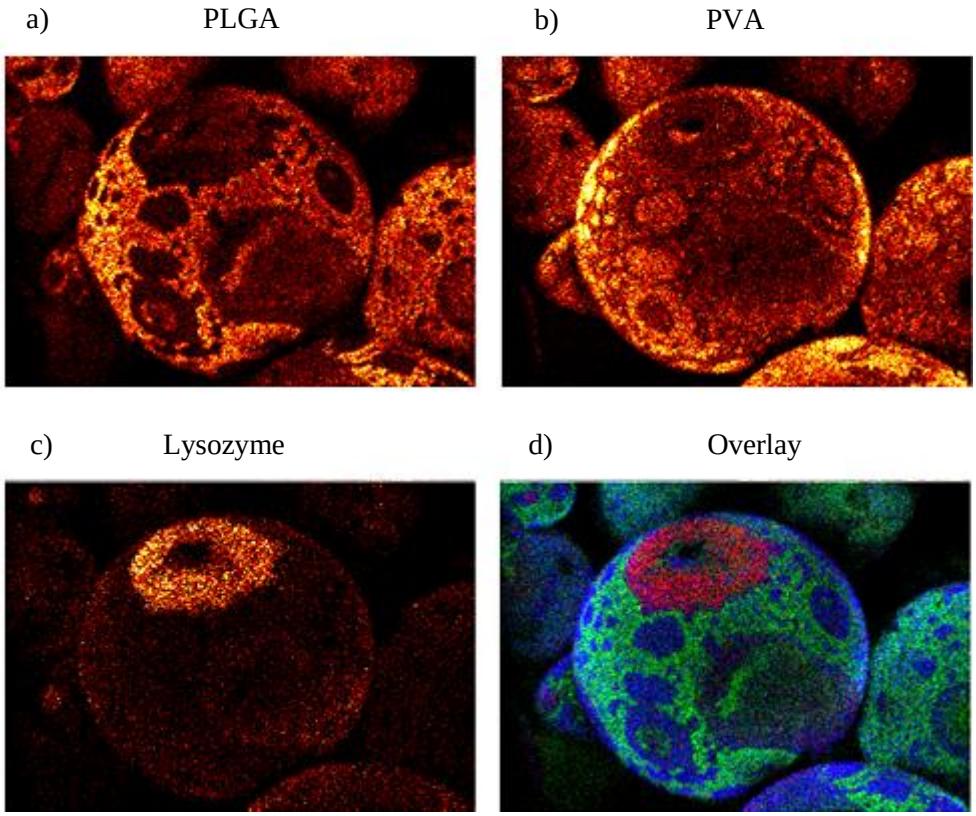

Figure 5.5 ToF-SIMS imaging of the surface of a microsphere measuring 149 µm in diameter showing the secondary ion image generated from the diagnostic anions identified within the ToF-SIMS spectra, for a) PLGA (*m/z* 71/73 and 87/89), b) PVA (*m/z* 59), c) lysozyme (*m/z* 26 and 42) and d) an overlay showing PLGA (green), PVA (blue) and lysozyme (red).

Further representative ToF-SIMS images of microspheres ranging in size from 47 to 169 µm in diameter are demonstrated in Figure 5.6. All microspheres analysed again show a patchy discontinuous surfactant film at the surface of the microspheres and also the degree of coverage appears to be comparable between microspheres analysed. The surface lysozyme is again found primarily as highly intense circular ring-like structures surrounding near-surface pores.

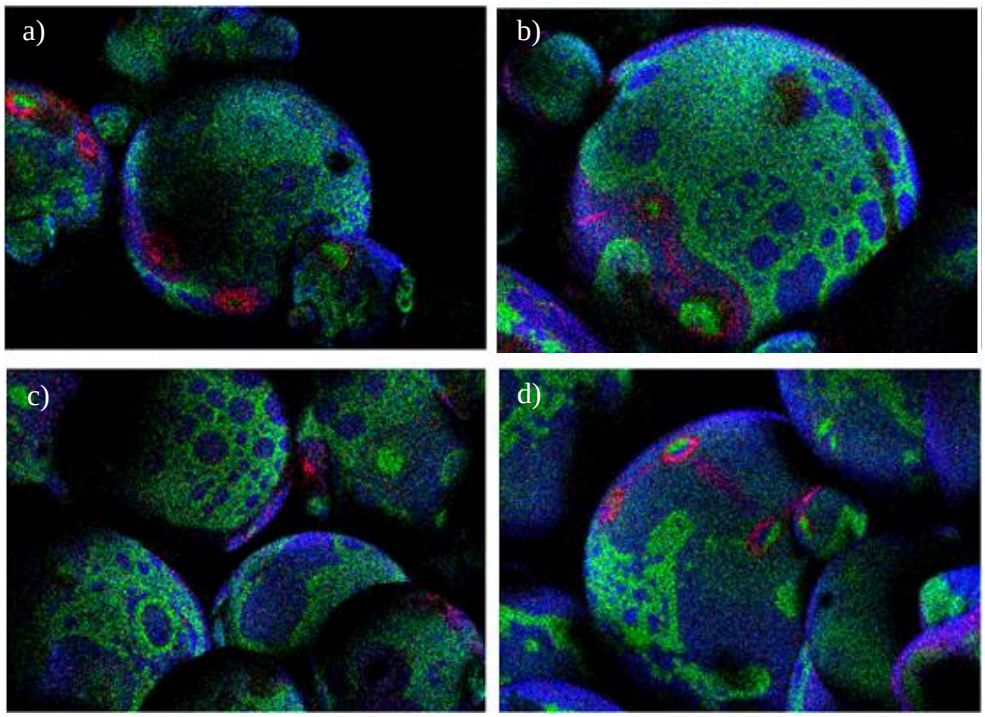

Figure 5.6 ToF-SIMS surface analysis of a range of w/o/w microspheres showing an overlay of PLGA (green), PVA (blue) and lysozyme (red).

ToF-SIMS sputtering and AFM analysis were applied to the surface of the microspheres in order to rationalise the thickness of the surfactant layer presented in Figure 5.7. Figure 5.7a-d shows the surface of a microsphere which has been exposed to increasing sputtering with C_{60}^{2+} primary ions. The central microsphere focussed on measures 172 µm in diameter and is shown before sputtering in Figure 5.7a. Two pores are clearly visible at the surface in addition to fissures at the surface, one pore appearing empty and one rich in lysozyme. The characteristic discontinuous PVA layer is present at the surface and a diffuse distribution of lysozyme in regions rich with PVA is also observed, further suggesting a relationship between the spread of PVA and lysozyme at the surface. After the initial 28 s of sputtering shown in Figure 5.7b, it is apparent the PVA surfactant layer is being eroded and extremely thin, with much of it being removed from the right side of the image where sputtering is most effective revealing the PLGA substrate immediately beneath this layer. The revealed PLGA surface confirms the presence of PVA as an overlayer at the surface of the microspheres and not a surface feature of the PLGA itself. The ion intensity of the

diffuse surface lysozyme is also reduced and it is gradually apparent that with sputtering the origin of the surface lysozyme is related to the surface pores present including one pore which is labelled that was not clearly visible in Figure 5.7a. On further sputtering shown in Figure 5.7c and 5.7d, the PVA layer is removed and it is clear one pore in particular is enriched with protein, however there are residual low intensity lysozyme signals from within other surface pores. It should be noted that the topography of the microspheres and primary ion beams being 180° from one another does not allow sputtering to remove the PVA and lysozyme from the entire surface of the central microsphere focussed on (see upper top and left edge) in Figure 5.7a-d. However the microsphere at the top left of the image has been effectively sputtered which highlights field line effects in ToF-SIMS topography [35].

The secondary electron imaging of the ToF-SIMS, shown in Figure 5.7e, illustrates the surface structures visible in the SIMS images and shows a thin fissure between three surface pores which has also been imaged with the high lateral resolution capable with ToF-SIMS.

AFM shown in Figure 5.7f was applied to the top of a microsphere before sputtering for 100 s then again to the same microsphere after sputtering shown in Figure 5.7g. A thin smooth discontinuous overlayer is observed on all microspheres analysed before sputtering. Line analysis of the overlayer thickness across all data obtained shows an average overlayer thickness of 4.54 ± 0.75 nm. Figure 5.7f shows areas with a continuous film and the centre has a region of random shaped island features which appear to have an equivalent height and form to the larger overlayer. After sputtering as shown in Figure 5.7g it is confirmed this layer is removed in its entirety and that it is preferentially sputtered leaving the rougher PLGA visible (Rq of 1.83 nm before and 3.31 nm after sputtering of the PVA surfactant layer.) The line scans shown also indicate the PLGA surface has more prominent craters after sputtering than are visible beforehand, this is likely in part due to the effect of prolonged ion bombardment of the microsphere surface.

In previous work by Shard *et al.* on sputtering of PLA, it was demonstrated that the C_{60} ion dose applied in this work is consistent with 4 nm of PLA removed per sputtering cycle[36]. While this value may change depending on the polymeric material examined, it provides a useful benchmark for organic polymers. Interestingly, the thickness of 4.5 nm of the PVA layer as determined by AFM correlates well with the sputtering data and also the work of Shard et al.[36] In summary, the consistency of the overlayer thickness and the thickness of the smaller islands of discontinuous surfactant observed in Figure 5.7f suggests a 4.5 nm thick PVA monolayer which remains after drying. The dynamic equilibrium model of PVA adsorbing and leaving the surface of the microspheres could explain the patchy morphology shown[37].

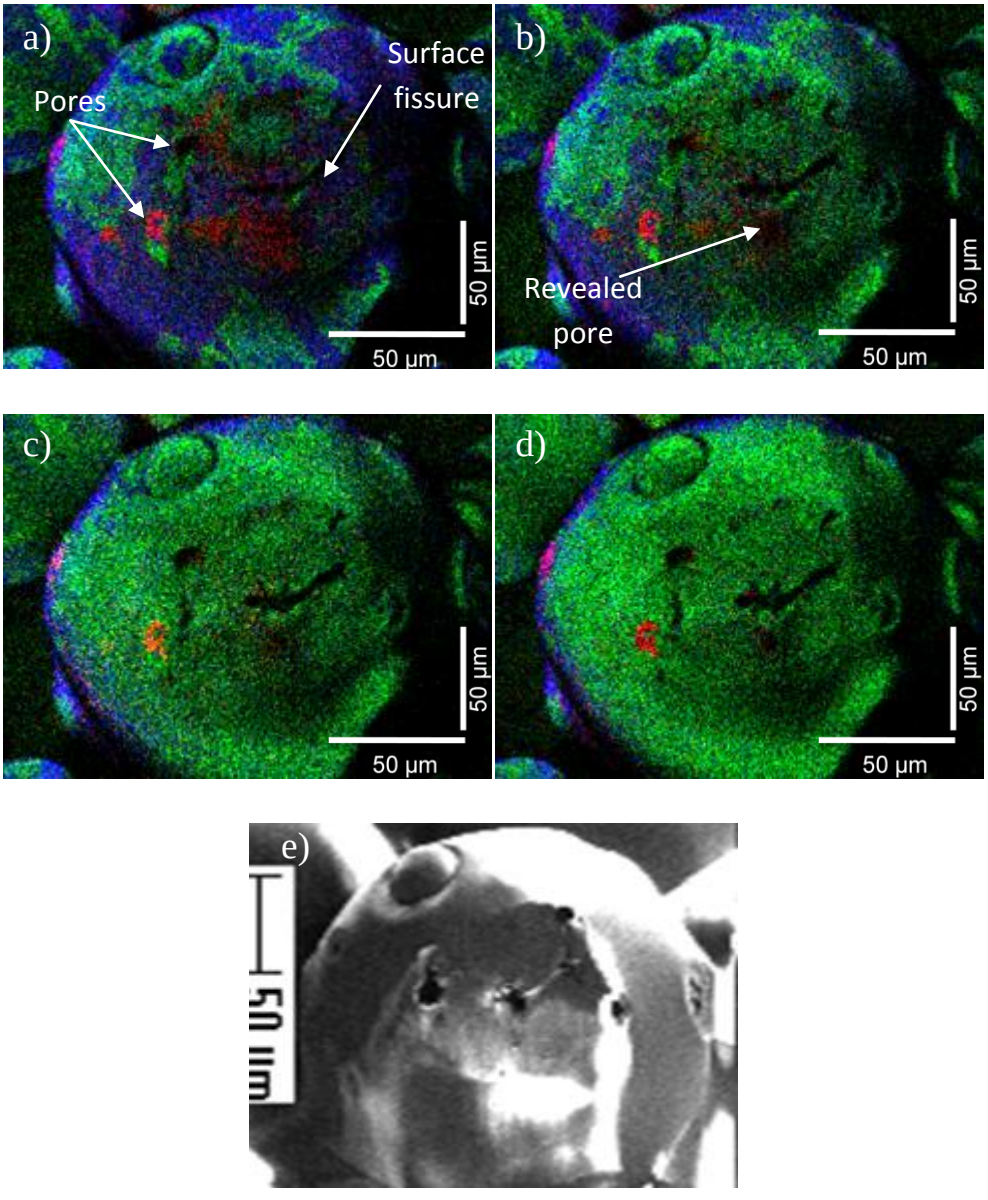

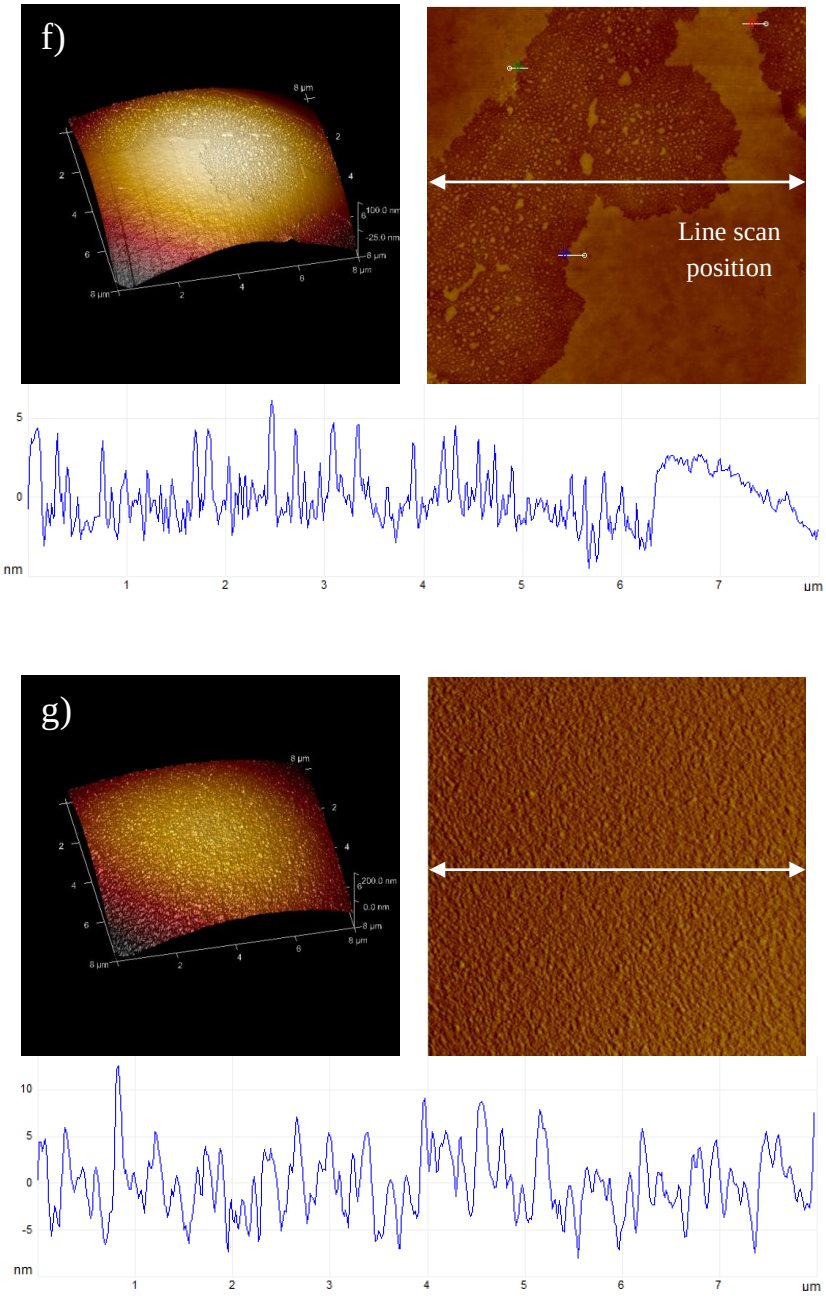

Figure 5.7 a) ToF-SIMS of a microsphere before sputtering b) after 28 s, c) 56 s and d) 84 s of sputtering. e) Secondary electron image of the resulting microsphere. f) AFM height image 1st order plane fitted of an 8 µm^2 area at the top of a microsphere before and g) after sputtering. Corresponding 3rd order flattened AFM height images, and a line scan (indicated) are also shown.

Confocal Raman mapping was applied to provide a 3D understanding of the organisation of components across the surface and also within the bulk of the microspheres shown in Figure 5.8. Confocal Raman analysis is feasible in this case due to the optical transparency of PLA. The confocal Raman map of a single optical slice in Figure 5.8a shows the presence of pores ranging in size within the bulk of the microsphere represented typically as black (indicating void space) or red (indicating lysozyme) spherical areas within the PLGA microsphere which is represented in green. These pores appear to range from 2 to 16 μm in diameter. The larger pores shown in Figure 5.8a and b appear to be largely devoid of material within the centre. Conversely the smaller pore features are filled with protein that consistently measure approximately 2 μm in diameter. This image is typical of all the microsphere structures observed. Such pores are formed during the inversion step of the double emulsion production method however the heterogeneous sizing, and distribution of protein within the pores suggests a complex mechanism is responsible for the distribution of components in the w/o/w system as shown by confocal Raman[38].

A protein coating is found adsorbed to the oil phase PLGA interface within some of the large pores. The thickness of this layer is variable as well as the coverage. Figure 5.8b provides an interpolated 3D representation generated using confocal Raman maps taken at 1 μm intervals in the z-axis and the 1 μm depth resolution allows for mathematical interpolation. This representation shows the protein distribution around a large pore which contains a significant concentration of protein adsorbed to the PLGA interface. It is apparent that the small pores are generally found in close proximity to the larger pores.

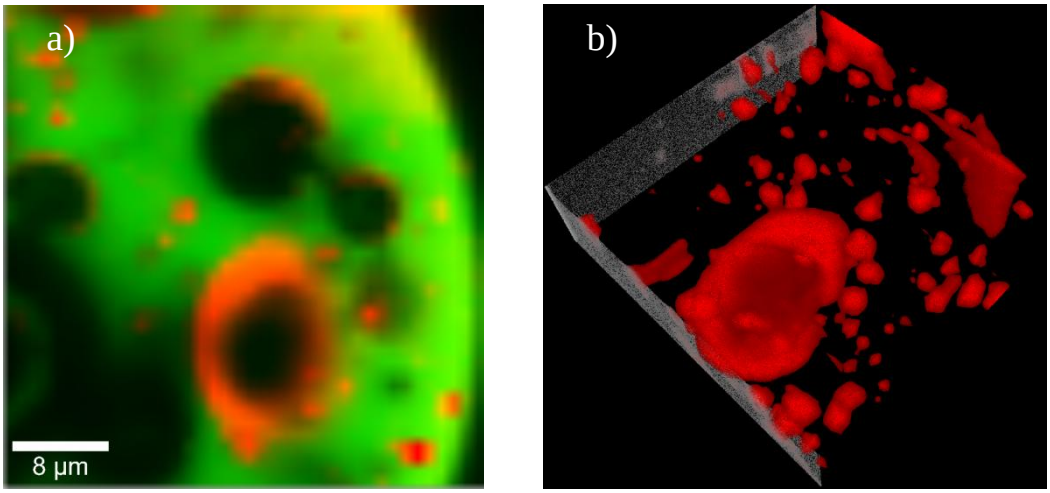

Figure 5.8 a) A confocal Raman map indicating PLGA as green and lysozyme as red, showing large pores, void spaces and protein adsorbed to the wall of the pore and concentrated pores measuring ~2 µm in diameter. b) An interpolated 3D representation of the protein distribution within a 40 μm^2 area of a microsphere showing from 20 µm (top of image) to 30 µm (bottom of image) of the microsphere bulk.

ToF-SIMS analysis of sectioned microspheres was undertaken to resolve the chemistry of the bulk of the microspheres shown in Figure 5.9. Figure 5.9c shows an overlay of lysozyme (red), PLGA (green) and PVA distribution (blue) in this cross section. Pore features ranging in size from 2 µm to 18 µm in diameter are observed, which is comparable with the values determined by the confocal Raman analysis. Naturally, the maximum diameter of any pore feature may lie above or below the point of the cross section but both the confocal Raman and ToF-SIMS data illustrates the diversity in size and composition of the pores. When comparing Figure 5.9a and b, lysozyme is clearly evident in some pores within the microsphere bulk. Again, it is present as dense cluster of protein in the smaller pore features and it appears to cover the surface interface with the PLGA in some of the larger pores. The PVA visible as noted in Figure 5.9c in one pore found in the bottom right of the image was a rare occurrence in the data collected suggesting this morphology is not a common feature, and the same pore also contains lysozyme, showing drug to be encapsulated within.

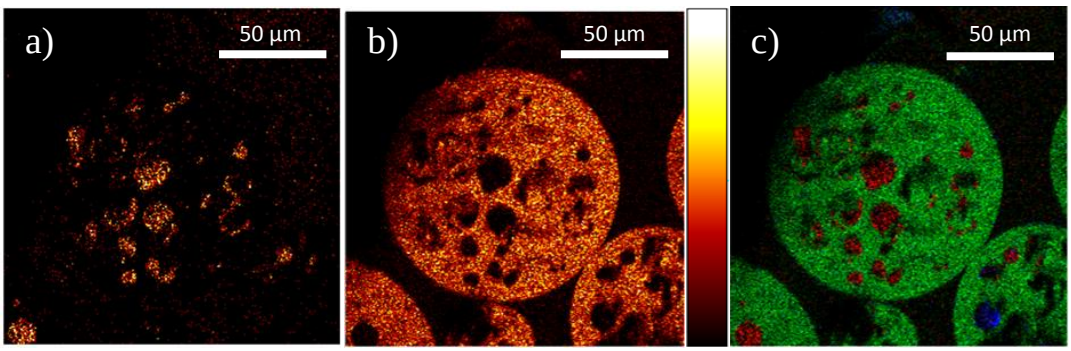

Figure 5.9 ToF-SIMS of a sectioned microsphere showing a) lysozyme (CNO^-), b) PLGA ($C_3H_3O_2^-$,$C_3H_5O_2^-$, $C_3H_3O_3^-$ & $C_3H_5O_3^-$), and c) an overlay showing lysozyme (red), PLGA (green) and PVA ($C_2H_3O_2^-$ blue).

ToF-SIMS analysis has shown many pores contain a larger concentration of lysozyme within the cross section whereas confocal Raman analysis has shown what is being imaged in the large pores is protein at the edges and base represented as a flat 2D image, illustrating the complementary data generated by the high surface specificity and resolution of ToF-SIMS and the understanding of the 3D distribution of constituents achieved with confocal Raman mapping.

The comprehensive analysis of the PLGA lysozyme system illustrates the potential for understanding the distribution of the protein and surfactant within the complex architecture of the microparticles formed from a multiple emulsion system. The visualisation of the surfactant layer on the surface of the microparticles is particularly notable. Traditionally measurements of surfactant concentration have relied on the zeta potential (measuring the electric potential in an interfacial double layer) to approximate the variation in surfactant at the surface[39]. SIMS has shown its utility in providing high resolution chemical images of this system. Surfactant is present as a discrete but laterally incomplete layer, ToF-SIMS and AFM are able to chemically and physically visualise respectively the integrity and fractal pattern of the surfactant across the surface of the particles. The PLGA particles are formed in an excess of PVA and hence the detection of a complete homogenous PVA surface layer was initially expected. An effective PVA coating would be required to stabilize the microparticle formation in solution and on evaporation of the organic solvent[40]. Indeed, the surfactant

concentration optimisation has an important role in reducing the diameter[41, 42] of the resulting microspheres through stabilisation of the emulsion droplets, reducing the occurrence of coalescence and allowing for a greater number of droplets to be encapsulated[43]. One possible explanation of the visualisation of the incomplete PVA coverage on the microparticle surface may be due to the contraction of the film during the drying process. Interestingly, the thickness of the PVA layer was largely uniform where it existed across the surface as measured by AFM and sputtering ToF-SIMS studies. This approach has shown it is possible to visualise the surface surfactant distribution at nm resolution that may provide a new method for future experimentation to correlate *in vitro* performance with surfactant coverage.

The studies presented in this chapter show that the protein on the surface of the microparticles is organised in a number of ways: firstly, the majority of the surface protein appears to be densely clustered around features that are associated with sub-surface protein filled pores that touch the outer surface of the microparticles due to incomplete encapsulation of the protein rich water droplets in the particle formation process. The ToF-SIMS images show intense signals, located often in ring around open pores or ribbon structures traversing across the microparticle surfaces. Secondly, there is evidence for the presence of protein dispersed within the surfactant film layer itself. This work represents the first example where the spatial location of the protein, surfactant and the polymer substrate in the ToF-SIMS images of the microparticle surfaces has been demonstrated.

With regard to the bulk distribution of the protein within the microparticles, confocal Raman analysis of the intact particles and the ToF-SIMS imaging of the microtomed particles confirm that lysozyme is located in the pores formed by the evaporation of water from the aqueous droplets dispersed within the PLA rich organic phase. The wide size distribution of these pores suggests incomplete stabilisation of the water droplets by the PVA surfactant, the larger ones potentially being formed via coalescence of the droplets during the removal of solvent during the particle production process[44]. The internal contents of microemulsion droplets are known to diffuse and undergo collisions, should these

collisions be sufficiently energetic the surfactant film may rupture causing droplet exchange which may explain the size distribution[45]. Both the Raman and ToF-SIMS analysis show the presence of a population of smaller pores (2-5 μm) dispersed throughout the microparticles which are protein rich. In contrast, protein is coating the inner surface of the larger pores (up to 20 μm) leaving larger volume unoccupied. The mechanism for the formation of such void spaces is unclear in the latter case but the potential coalescence of protein rich water droplets during the particle production may play a role as the subsequent removal of water at the droplet interface would promote the transport of the protein with this solvent front to the surface of the pore. This analysis has revealed a complex and heterogeneous organisation of protein distribution within the microparticle bulk that may have an impact on the mechanism and kinetics of release of the protein from such systems.

5.4 Conclusion

Partially porous protein loaded microspheres for use as controlled drug delivery biomaterials have had their surface and bulk scrutinised with an array of complementary analytical techniques. For the first time the ability to spatially image PVA surfactant and protein adsorbed to the surface of microspheres using ToF-SIMS imaging has been shown and that this surfactant layer has a thickness of circa 4 nm which can be removed under ToF-SIMS sputtering studies which is confirmed by AFM. The ability to spatially map the surface and bulk microparticles prepared by the double emulsion approach has revealed that distribution of the lysozyme to be complex and heterogeneous. This combined approach of using the analytical techniques of ToF-SIMS (imaging and sputtering), confocal Raman, AFM and other complimentary methodologies provides a powerful toolset for the study of the spatial chemical distribution of biomolecules and excipients such as surfactants within controlled release formulations such as microparticles. The high lateral resolution in ToF-SIMS imaging achieved providing valuable characterisation results, fulfilling an aim of this thesis. The techniques utilised have been shown to be highly complementary for the characterisation of controlled release injectables and by association, implantable formulations, increasing the understanding of the influence of the

fabrication process and formulation composition on the properties of the resulting delivery systems. This work is a culmination of the expertise gained throughout the chapters of this thesis and demonstrates the real world benefit which can be achieved through the improved understanding of such biomedically relevant formulations.

5.5 References

1. Grenha, A., B. Seijo, C. Serra, and C. Remunan-Lopez, *Biomacromolecules*, 2007. **8**(7): p. 2072-2079.
2. Chesko, J., J. Kazzaz, M. Ugozzoli, M. Singh, D.T. O'Hagan, C. Madden, M. Perkins, and N. Patel, *Journal of Pharmaceutical Sciences*, 2008. **97**(4): p. 1443-1453.
3. Dai, C.Y., B.C. Wang, and H.W. Zhao, *Colloids and Surfaces B-Biointerfaces*, 2005. **41**(2-3): p. 117-120.
4. Koneracka, M., M. Muckova, V. Zavisova, N. Tomasovicova, P. Kopcansky, M. Timko, A. Jurikova, K. Csach, V. Kavecansky, and G. Lancz, *Journal of Physics-Condensed Matter*, 2008. **20**(20).
5. Grenha, A., B. Seijo, and C. Remuñán-López, *European Journal of Pharmaceutical Sciences*, 2005. **25**(4-5): p. 427-437.
6. Men, Y., C. Thomasin, H.P. Merkle, B. Gander, and G. Corradin, *Vaccine*, 1995. **13**(7): p. 683-689.
7. Singh, M., M. Briones, G. Ott, and D. O'Hagan, *Proceedings of the National Academy of Sciences of the United States of America*, 2000. **97**(2): p. 811-816.
8. O'Hagan, D., M. Singh, M. Ugozzoli, C. Wild, S. Barnett, M.C. Chen, M. Schaefer, B. Doe, G.R. Otten, and J.B. Ulmer, *Journal of Virology*, 2001. **75**(19): p. 9037-9043.
9. Okada, H., *Advanced Drug Delivery Reviews*, 1997. **28**(1): p. 43-70.
10. Bolla, M., D. Gonzalez, P. Warde, J.B. Dubois, R.O. Mirimanoff, G. Storme, J. Bernier, A. Kuten, C. Sternberg, T. Gil, L. Collette, and M. Pierart, *New England Journal of Medicine*, 1997. **337**(5): p. 295-300.
11. Kotake, T., M. Usami, H. Akaza, K. Koiso, Y. Homtna, K. Kawabe, Y. Aso, S. Orikasa, J. Shimazaki, S. Isaka, O. Yoshida, Y. Hirao, E. Okajima, S. Naito, J. Kumazawa, H. Kanetake, Y. Saito, Y. Ohi, Y. Ohashi, and Z.S. Group, *Japanese Journal of Clinical Oncology*, 1999. **29**(11): p. 562-570.
12. Kemp, S.F., P.J. Fielder, K.M. Attie, S.L. Blethen, E.O. Reiter, K.M. Ford, M. Marian, L.N. Dao, H.J. Lee, and P. Saenger, *Journal of Clinical Endocrinology & Metabolism*, 2004. **89**(7): p. 3234-3240.
13. Sinha, V.R. and A. Trehan, *Critical Reviews in Therapeutic Drug Carrier Systems*, 2005. **22**(6): p. 535-602.
14. Davies, M.C., A. Brown, J.M. Newton, and S.R. Chapman, *Surface and Interface Analysis*, 1988. **11**(12): p. 591-595.
15. Scholes, P.D., A.G.A. Coombes, L. Illum, S.S. Davis, J.F. Watts, C. Ustariz, M. Vert, and M.C. Davies, *Journal of Controlled Release*, 1999. **59**(3): p. 261-278.
16. Belu, A.M., M.C. Davies, J.M. Newton, and N. Patel, *Analytical Chemistry*, 2000. **72**(22): p. 5625-5638.
17. Mahoney, C.M., D.V. Patwardhan, and M.K. McDermott, *Applied Surface Science*, 2006. **252**(19): p. 6554-6557.
18. Belu, A., C. Mahoney, and K. Wormuth, *Journal of Controlled Release*, 2008. **126**(2): p. 111-121.
19. Fisher, G.L., A.M. Belu, C.M. Mahoney, K. Wormuth, and N. Sanada, *Anal Chem*, 2009. **81**(24): p. 9930-40.

20. Shakesheff, K.M., M.C. Davies, D.E. Jackson, C.J. Roberts, S.J.B. Tendler, V.A. Brown, R.C. Watson, D.A. Barrett, and P.N. Shaw, *Surface Science*, 1994. **304**(1-2): p. L393-L399.
21. Mu, L. and S.S. Feng, *Journal of Controlled Release*, 2001. **76**: p. 239-254.
22. Yang, C.M., D. Plackett, D. Needham, and H.M. Burt, *Pharmaceutical Research*, 2009. **26**(7): p. 1644-1656.
23. van Manen, H.J., A.A. van Apeldoorn, R. Verrijk, C.A. van Blitterswijk, and C. Otto, *International Journal of Nanomedicine*, 2007. **2**(2): p. 241-252.
24. Balss, K.M., G. Lianos, G. Papandreou, and C.A. Maryanoff, *Journal of Biomedical Materials Research Part A*, 2008. **85A**(1): p. 258-270.
25. Szostak, R. and S. Mazurek, *Analyst*, 2002. **127**(1): p. 144-148.
26. Mazurek, S. and R. Szostak, *Journal of Pharmaceutical and Biomedical Analysis*, 2008. **48**(3): p. 814-821.
27. Sasic, S., D.A. Clark, J.C. Mitchell, and M.J. Snowden, *Analyst*, 2004. **129**(11): p. 1001-1007.
28. Zhang, L., M.J. Henson, and S.S. Sekulic, *Analytica Chimica Acta*, 2005. **545**(2): p. 262-278.
29. Whitaker, M.J., R.A. Quirk, S.M. Howdle, and K.M. Shakesheff, *Journal of Pharmacy and Pharmacology*, 2001. **53**(11): p. 1427-1437.
30. Hou, Q.P., P.A. De Bank, and K.M. Shakesheff, *Journal of Materials Chemistry*, 2004. **14**(13): p. 1915-1923.
31. Kempen, D.H.R., L. Lu, T.E. Hefferan, L.B. Creemers, A. Maran, K.L. Classic, W.J.A. Dhert, and M.J. Yaszemski, *Biomaterials*, 2008. **29**(22): p. 3245-3252.
32. Cohen, S., T. Yoshioka, M. Lucarelli, L.H. Hwang, and R. Langer, *Pharmaceutical Research*, 1991. **8**(6): p. 713-720.
33. Ravi, S., K.K. Peh, Y. Darwis, B.K. Murthy, T.R.R. Singh, and C. Mallikarjun, *Indian Journal of Pharmaceutical Sciences*, 2008. **70**(3): p. 303-309.
34. Shard, A.G., M.C. Davies, Y.X. Li, C. Volland, and T. Kissel, *Macromolecules*, 1997. **30**(10): p. 3051-3057.
35. Lee, J.L.S., I.S. Gilmore, I.W. Fletcher, and M.P. Seah, *Applied Surface Science*, 2008. **255**(4): p. 1560-1563.
36. Shard, A.G., P.J. Brewer, F.M. Green, and I.S. Gilmore, *Surface and Interface Analysis*, 2007. **39**(4): p. 294-298.
37. Moorkanikkara, S.N. and D. Blankschtein, *Langmuir*, 2009. **25**(11): p. 6191-6202.
38. Bohmer, M.R., J.A.M. Steenbakkers, and C. Chlon, *Colloids Surf B Biointerfaces*, 2010. **79**(1): p. 47-52.
39. Davies, O.R., L. Head, D. Armitage, E.A. Pearson, M.C. Davies, M. Marlow, and S. Stolnik, *Langmuir*, 2008. **24**(14): p. 7138-7146.
40. Bouissou, C., J.J. Rouse, R. Price, and C.F. van der Walle, *Pharmaceutical Research*, 2006. **23**(6): p. 1295-1305.
41. Liu, Y. and X.M. Deng, *Journal of Controlled Release*, 2002. **83**(1): p. 147-155.
42. De Rosa, G., R. Iommelli, M.I. La Rotonda, A. Miro, and F. Quaglia, *Journal of Controlled Release*, 2000. **69**(2): p. 283-295.
43. Heiskanen, H., P. Denifl, M. Hurme, and P. Pitkanen, *Chemical Engineering & Technology*, 2010. **33**(10): p. 1635-1644.

44. Rosca, I.D., F. Watari, and M. Uo, *Journal of Controlled Release*, 2004. **99**(2): p. 271-280.
45. Fletcher, P.D.I., A.M. Howe, and B.H. Robinson, *Journal of the Chemical Society-Faraday Transactions I*, 1987. **83**: p. 985-1006.